

Quasi-normal modes and Hawking radiation of a charged Weyl black hole

Guoyang Fu^{1,*}, Dan Zhang^{2,†}, Peng Liu^{3,‡}, Xiao-Mei

Kuang^{1,4,§}, Qiyuan Pan^{2,¶} and Jian-Pin Wu^{1,4,**}

¹ *Center for Gravitation and Cosmology,*

College of Physical Science and Technology,

Yangzhou University, Yangzhou 225009, China

² *Key Laboratory of Low Dimensional Quantum*

Structures and Quantum Control of Ministry of Education,

Synergetic Innovation Center for Quantum Effects and Applications,

and Department of Physics, Hunan Normal University, Changsha, Hunan 410081, China

³ *Department of Physics and Siyuan Laboratory,*

Jinan University, Guangzhou 510632, P.R. China and

⁴ *Shanghai Frontier Science Center for Gravitational Wave Detection,*

Shanghai Jiao Tong University, Shanghai 200240, China

Abstract

We study the scalar field system over a charged Weyl black hole, which is depicted by a parameter λ . Under the perturbation of scalar field, the system is unstable for zero angular number, but stable for non-zero one. We are specially interested in the properties of QNM spectra, dynamical evolution and Hawking radiation for the modes with non-zero angular number, which discloses some peculiar properties of this charged Weyl black hole. What is remarkable is that an exponential decay obviously emerges in the phase of the ringing tail as λ increases. It indicates that the characteristic parameter λ has an obvious imprint on the ringing tail, which is expected to be detected by future observations. Other effects of the parameter λ on the QNM spectra, dynamical evolution and Hawking radiation have also been explored.

*FuguoyangEDU@163.com

†danzhanglnk@163.com

‡phylp@email.jnu.edu.cn

§xmeikuang@yzu.edu.cn

¶panqiyuan@hunnu.edu.cn

**jianpinwu@yzu.edu.cn

Contents

I. Introduction	2
II. Massless scalar field over charged Weyl black hole	4
III. Quasi-normal modes	7
IV. Dynamical evolution	10
V. Grey-body factor and energy emission rate	12
VI. Conclusion and discussion	15
Acknowledgments	16
A. WKB method and error estimation	16
References	19

I. INTRODUCTION

Recent observations of gravitational waves (GWs) from the coalescence of binary systems [1–3] and shadows of supermassive black holes (M87* and SgrA*) by the Event Horizon Telescope (EHT) [4–7] confirm the existence of black hole and thus test the robustness of general relativity (GR). Nonetheless, there are still numerous open fundamental questions, including quantum gravity, dark energy and dark matter problems, and so on. These unresolved problems have spurred a renewed interest in the gravity theories beyond GR, especially, their effects deviating from GR could have possible prints in the detected GWs and black hole shadows.

An interesting modified gravity theory is the Weyl gravity. It is a fourth-order gravity theory, originally proposed by H. Weyl [8]. Since the Weyl gravity is power-counting renormalizable [9, 10], it is a suitable candidate to construct quantum gravity theory [11, 12]. This theory is also a possible UV completion of GR. It’s worth pointing out that there is an equivalence between GR and Weyl gravity with the Neumann boundary conditions [13, 14].

Specifically, the action of the Weyl gravity is [8, 15]

$$S = -\kappa \int d^4x \sqrt{-g} C_{\mu\nu\rho\sigma} C^{\mu\nu\rho\sigma}, \quad (1)$$

where κ is the coupling constant. The Weyl tensor

$$C_{\mu\nu\rho\sigma} = R_{\mu\nu\rho\sigma} + \frac{R}{6}(g_{\mu\rho}g_{\nu\sigma} - g_{\mu\sigma}g_{\nu\rho}) - \frac{1}{2}(g_{\mu\rho}R_{\nu\sigma} - g_{\mu\sigma}R_{\nu\rho} - g_{\nu\rho}R_{\mu\sigma} + g_{\nu\sigma}R_{\mu\rho}), \quad (2)$$

is invariant under the local conformal transformation $\tilde{g}_{\mu\nu} = \Omega^2 g_{\mu\nu}$, where Ω is a function of the local spacetime point. Such transformation preserves the angles but not the distances. A static and spherically symmetric vacuum black hole solution from Weyl gravity is worked out in [16]. Of particular interest is that it can address both the dark energy related phenomena [17, 18] and the dark matter scenario [16]. Further, the general Reissner-Nordström (RN), Kerr and Kerr-Newman solutions are also obtained in [19].

More recently, an alternative black hole solution from Weyl gravity has been constructed with the use of the background field method and linear approximation [20]. With this inspiration, a charged Weyl black hole has also been proposed in [21]. This charged solution can be reformed into a RN-like metric, but the sign in the ‘charge’ term is minus instead. Thus, here we have great interest in disclosing the characterized features of such a RN-like black hole in Weyl gravity.

It is well known that one powerful way to extract the black hole characterization is to perturb it and then see how it responds. The physics after perturbing a black hole is complex, but we know that it will result in the radiation of GWs, and before the system relaxes to be equilibrium, there exists the black hole merger phase in which the excitation of other matter fields can occur. This stage is known as the ringdown phase, and in this phase the black hole emits the GWs with the characteristic discrete frequencies, dubbed the quasi-normal modes (QNMs) frequencies which encode the decaying scales and damped oscillating frequencies [22]. More importantly, the QNM spectra of the matter fields also depend on the background spacetime. It is expected that any deviation from GR has an imprint on the QNM spectra, thus serving as a specific probe of modified gravity [23, 24]. Given all that, as the first step toward understanding the properties of this charged Weyl black hole, we consider a probe massless scalar field over this background and study the properties of its QNM spectra.

We are also interested in the Hawking radiation, as a quantum effect, which could partly describe the near horizon nature of a black hole [25]. It is well known that the Hawking

radiation is not ideal black body since the particles created in the vicinity of event horizon without enough energy can not penetrate the potential barrier. So only part of the particles can be observed at infinity and the radiation behaves as a grey body. This process make the radiation be a scattering problem. Thus, we can just solve the wave equation outside the black hole and calculate the scattering coefficient which could further give us the grey-body factor as well as the energy radiation rate. Lots of works on the Hawking emission spectra in GR, modified gravity theory, and in the analogue gravity theory, which is aimed at testing the Hawking radiation in the laboratory, have been widely explored to further understand the features of the black holes (see for example [26–36]).

Our paper is organized as what follows. In section II, we briefly review the charged Weyl black hole solution and analyze the instability of this black hole under the scalar field perturbation. Section III and section IV are respectively dedicated to the properties of the QNM spectra and the dynamical evolution of the scalar field. Furthermore, section V focuses on the grey-body factor and energy emission rate. In section VI, we present the conclusions and discussions. In addition, we also give a brief introduction on the WKB method in appendix A.

II. MASSLESS SCALAR FIELD OVER CHARGED WEYL BLACK HOLE

The RN-like solution of Weyl gravity in the presence of a charged source is given by [21]

$$ds^2 = -B(r)dt^2 + \frac{dr^2}{B(r)} + r^2(d\theta^2 + \sin^2\theta d\phi^2), \quad (3)$$

with

$$B(r) = 1 - \frac{r^2}{\lambda^2} - \frac{Q^2}{4r^2}, \quad (4)$$

where λ and Q are the black hole parameters. The second term r^2/λ^2 in the lapse function $B(r)$ is related to the dark energy scenario.

When $\lambda < Q$, a naked singularity is encountered. If $\lambda > Q$, the spacetime admits two horizons: the event horizon r_h and the cosmological horizon r_c , located at [37]

$$r_h = \lambda \sin \left(\frac{1}{2} \arcsin \left(\frac{Q}{\lambda} \right) \right), \quad (5)$$

$$r_c = \lambda \cos \left(\frac{1}{2} \arcsin \left(\frac{Q}{\lambda} \right) \right). \quad (6)$$

Then, we have the Hawking temeperature as

$$T_H = \frac{1}{\sqrt{2}\pi Q \lambda^{3/2}} \left(\lambda \sqrt{\lambda + \sqrt{\lambda^2 - Q^2}} - \frac{Q^2}{\sqrt{\lambda + \sqrt{\lambda^2 - Q^2}}} \right). \quad (7)$$

It is easy to find that when $\lambda = Q$, one has an extremal black hole, possessing a unique horizon at $r_{ex} = r_h = r_c = \lambda/\sqrt{2}$.

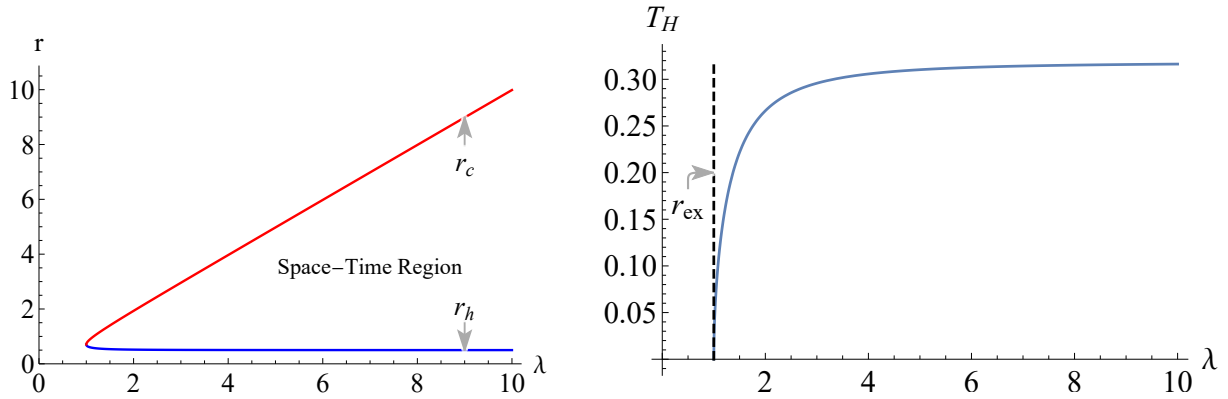


FIG. 1: Left plot: The horizon structure of the charged Weyl black hole for different λ . Right plot: The Hawking temeperature as the function of λ .

Through this paper, we shall set $Q = 1$ and leave λ free. Left plot in Fig.1 shows the horizon structure of this black hole for different λ . We clearly see that when $\lambda = Q = 1$, the cosmological horizon coincides with the event horizon. With λ growing larger, the spacetime region also becomes larger. We also show the Hawking temperature as the function of λ in the right plot in Fig.1. We find that the Hawking temperature increases with λ , and then approaches a constant as $\lambda \rightarrow \infty$, i.e., $T_H|_{\lambda \rightarrow \infty} = 1/\pi$.

Lots of works based on this black hole background have been widely explored, including the motion of massless particle, neutral massive particle, and electrically charged particle [37–40]. Here, we shall study the QNM spectra and the dynamical evolution of a massless scalar field over this black hole, and also its Hawking radiation which could help to further understand the properties of the black hole.

A probe massless scalar field ψ over the charged Weyl black hole can be described by the Klein-Gordon (KG) equation:

$$\frac{1}{\sqrt{-g}} \partial_\mu (\sqrt{-g} g^{\mu\nu} \partial_\nu \psi) = 0. \quad (8)$$

After making a separation of variables by a spherical harmonic $\psi = \Psi(t, r)Y_l(\theta, \phi)/r$, we can recast the KG equation into the Schrodinger-like form

$$-\frac{\partial^2 \Psi}{\partial t^2} + \frac{\partial^2 \Psi}{\partial r_*^2} - V(r)\Psi = 0, \quad (9)$$

where r_* is the tortoise coordinate defined as $dr_* = dr/B(r)$. $V(r)$ is the effective potential

$$V(r) = B(r) \left(\frac{l(l+1)}{r^2} + \frac{B'(r)}{r} \right). \quad (10)$$

Here l is the angular quantum number. This effective potential obviously depends on the black hole background as well as the angular quantum number.

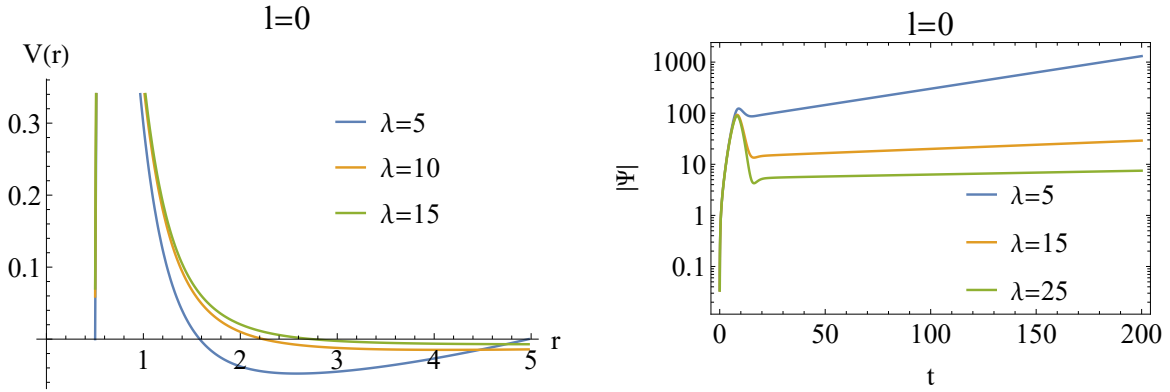


FIG. 2: Left plot: The potential $V(r)$ for $l = 0$ with different λ . Right plot: The evolution of the scalar field for $l = 0$ with different λ .

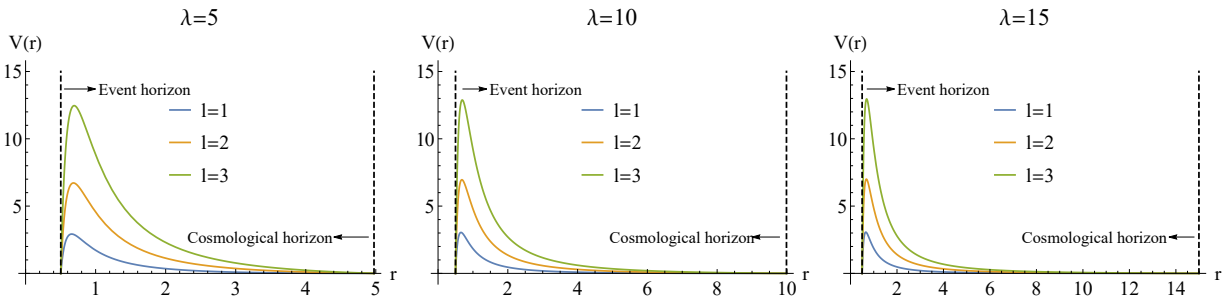


FIG. 3: The effective potential $V(r)$ for different l with fixed λ .

Left plot in Fig.2 shows the effective potential for $l = 0$ with different λ . A negative gap can be observed in the effective potential. Usually, the negative gap is a possible signal of instability. To proceed, we show the dynamical evolution of the scalar field in the right plot

in Fig.2¹. We find that the scalar field grows with time for any λ . It means that the system is unstable under the perturbation of the probe scalar field. We shall further confirm this point by the QNMs in Sec.III. While for $l > 0$, the effective potentials are always positive (Figs.3 and 4). It indicates that for $l > 0$, the system is stable under the perturbation of the scalar field.

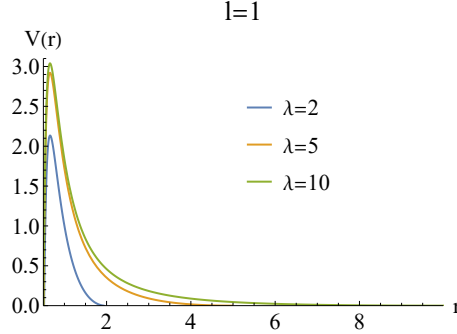


FIG. 4: The effective potentials for different λ with fixed $l = 1$.

Further, from Fig.3, we observe that for fixed black hole parameter λ , the height of the potential barrier increases with the increase of the angular quantum number, which is the universal properties of the potential barrier of black hole. For fixed l , we see that the height of the potential barrier grows with increasing λ (Fig.4) which also shows that the height increases slightly as λ is large enough. There is no doubt that the shape of the effective potential shall make a significant impact on the QNMs, dynamical evolution and Hawking radiation, which shall be illustrated in what follows.

III. QUASI-NORMAL MODES

QNMs are an intrinsic characteristic of the background spacetime, and therefore its spectra encode the key information about black holes [22, 41–44]. The nature of determining the QNMs is to solve the eigenvalue problem. There are several methods developed to determine the QNMs, among which the pseudospectral method is one of the powerful numerical tools. In this section, we shall implement pseudospectral method to calculate the QNM spectra. For the pseudospectral method, we can refer to [45] and also see [46–54] for the application

¹ We implement the dynamical evolution of the scalar field by the finite difference method (FDM), for which we shall give a brief introduction in Section IV.

in the calculation of QNMs in the black hole physics. We justify our findings by further cross-checking the results with the Wentzel-Kramers-Brillouin (WKB) method, which is a widely-used and well-understood method, and analyse the error between the WKB and pseudospectral methods. A brief introduction on the WKB method shall be presented in the appendix A.

The key point of the pseudospectral method is to discretize the differential equations and then solve the resulting generalized eigenvalue equations. Specially, we replace the continuous variables by a discrete set of collocation points called the grid points and expand the functions by some particular basis functions called cardinal functions. Usually, we use the Chebyshev grids and Lagrange cardinal functions

$$x_i = \cos\left(\frac{i}{N}\pi\right), \quad C_j(x) = \prod_{j=0, j \neq i}^N \frac{x - x_j}{x_i - x_j}, \quad i = 0, \dots, N. \quad (11)$$

Now we are ready to determine the QNM spectra. Let us first expand Ψ as $\Psi = e^{-i\omega t}\Phi$ such that we work in the frequency domain. Then, the KG equation takes the form

$$\frac{\partial^2 \Phi}{\partial r_*^2} + (\omega^2 - V(r))\Phi = 0. \quad (12)$$

There is an infinite but discrete set of eigenfrequencies ω_{ln} , where l is the angular momentum number and n its the overtone number characterizing the number of nodes of the radial solution. To calculate the QNM spectra, it is convenient to work in the Eddington-Finkelstein coordinate, where Eq.(12) is linear in the frequency ω . And then, one obtains the generalized eigenvalue equation as

$$(M_0 + \omega M_1)\Phi = 0, \quad (13)$$

where M_i ($i = 0, 1$) are the linear combination of the derivative matrices. The above equation can be solved directly by the Eigenvalue function in the Mathematica².

We present the QNM spectra as the function of λ in Fig.5. For $l = 0$, the real part of QNM spectrum is always zero. It indicates that there is no oscillation in the scalar field perturbation. While the imaginary part of QNM spectrum is always positive for all λ , which means that the perturbation grows and does not die out even in a long enough

² In order to solve Eq.(13), we need to impose the proper boundary conditions near the cosmological horizon. For more details, please refer to Ref.[46].

time. It suggests that the system is unstable under the scalar field perturbation, which is in agreement with the observation from the dynamical evolution of the scalar field shown in the right plot of Fig.2.

For $l > 0$, the imaginary part of the QNM spectrum is always negative and so the system is stable under the scalar field perturbation. It is consistent with the result of the potential shown in Fig.3. The absolute value of the real part of QNM spectrum increases with the increase of λ ³. It suggests that the oscillation of the dynamical perturbation increases with increasing λ . We also notice that both the real and imaginary parts of the QNM spectra approach a constant when λ is large enough. This observation is consistent with that the potential barrier, especially its height, is almost the same (only very small difference).

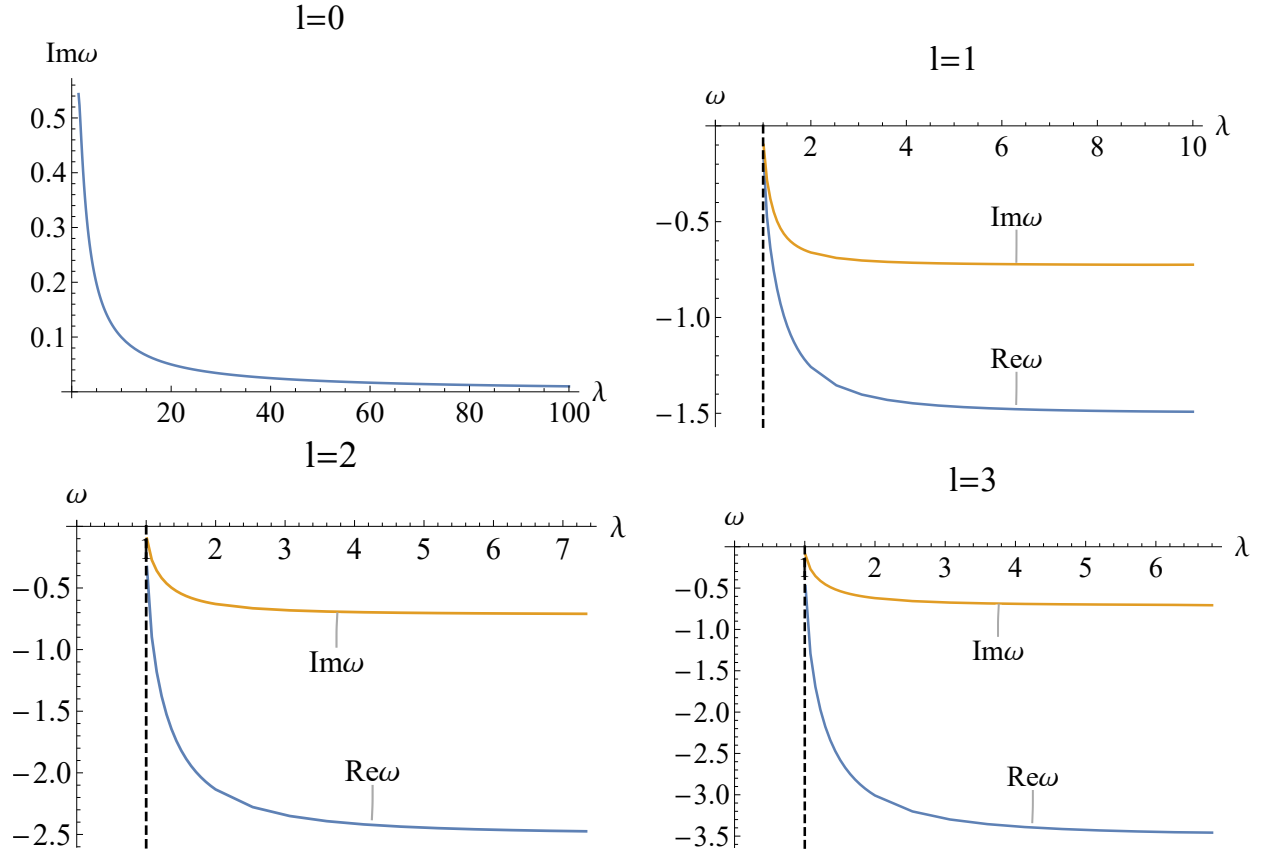


FIG. 5: The QNM spectra as the function of λ for different l . Notice that for $l = 0$, the real part of the QNMs is zero.

Finally, we show the QNM spectra with fixed λ for different angular number l and

³ The real part of the QNM spectrum is off axis and we only show the negative branch in Fig.5.

overtone number n by pseudospectral method and 6th order WKB method⁴ in Table III. The errors evaluated by $\delta\omega_{error} = |\omega_{PS} - \omega_{WKB_6}|/2$ between both two methods are also presented in this table. It is obvious that for fixed n , the errors decrease as l increases. It is consistent with the argument that the WKB formula usually gives a best accuracy for larger l ($l > n$)⁵.

n	l	PS	WKB ₆	$\delta\omega_{error}$
0	1	1.4650065-0.7187528i	1.4647270-0.718787i	0.000140805
	2	2.4447382-0.7028046i	2.4447097-0.702766i	0.0000238985
	3	3.4254973-0.6980106i	3.4254982-0.6980142i	$1.82346 * 10^{-6}$
1	1	1.1221779-2.3591926i	1.1198092-2.3710473i	0.00604452
	2	2.1875304-2.1898062i	2.1853061-2.1928363i	0.00187944
	3	3.2324728-2.1358198i	3.2322875-2.1359638i	0.00011733

TABLE I: The QNM spectra with $\lambda = 5$ for different angular number l and overtone number n by pseudospectral (PS) method and 6th order WKB (WKB₆) method.

IV. DYNAMICAL EVOLUTION

In this section, we shall explore the dynamical evolution of the massless scalar field for given initial perturbation. We are specially interested in the behaviors of the scalar field in the ringdown phase. The finite difference method (FDM) is a suitable approach to implement the dynamical evolution. Before proceeding, we briefly outline the key point of the FDM. For the details, we can refer to Refs.[57–59]. Firstly, we need to discretize the wave equation (9). The discretization scheme is to define $\Psi(r_*, t) = \Psi(j\Delta r_*, i\Delta t) = \Psi_{j,i}$ and $V(r(r_*)) = V(j\Delta r_*) = V_j$ (see the left plot in Fig.6 for the cartoon diagram of the discretization scheme of the coordinates (t, r_*)). Therefore, instead of the differential equation (9), we have the following difference equation

$$-\frac{(\Psi_{i+1,j} - 2\Psi_{i,j} + \Psi_{i-1,j})}{\Delta t^2} + \frac{(\Psi_{i,j+1} - 2\Psi_{i,j} + \Psi_{i,j-1})}{\Delta r_*^2} - V_j\Psi_{i,j} + \mathcal{O}(\Delta t^2) + \mathcal{O}(\Delta r_*^2) = 0. \quad (14)$$

⁴ We shall illustrate the choice of order of WKB method in appendix A.

⁵ See Refs.[55, 56] and also the discussions in appendix A.

Given the initial Gaussian distribution $\Psi(r_*, t < 0) = 0$ and $\Psi(r_*, t = 0) = \exp[-\frac{(r_* - a)^2}{2b^2}]$ with a and b being the constants, the iterate formula is derived as

$$\Psi_{i+1,j} = -\Psi_{i-1,j} + \frac{\Delta t^2}{\Delta r_*^2}(\Psi_{i,j+1} + \Psi_{i,j-1}) + (2 - 2\frac{\Delta t^2}{\Delta r_*^2} - \Delta t^2 V_j)\Psi_{i,j}. \quad (15)$$

The cartoon diagram of the iterative process of FDM is shown in the right plot in Fig.6. The Courant-Friedrichs-Lewy (CFL) condition for stability require $\Delta t/\Delta r_* < 1$. Here, we use $\Delta t/\Delta r_* = 0.5$. Actually, the numerical accuracy not only depends on the ratio of $\Delta t/\Delta r_*$, but also the respective values of Δt and Δr_* . Therefore, we must requires Δt and Δr_* to be small enough to satisfy the precision requirement.

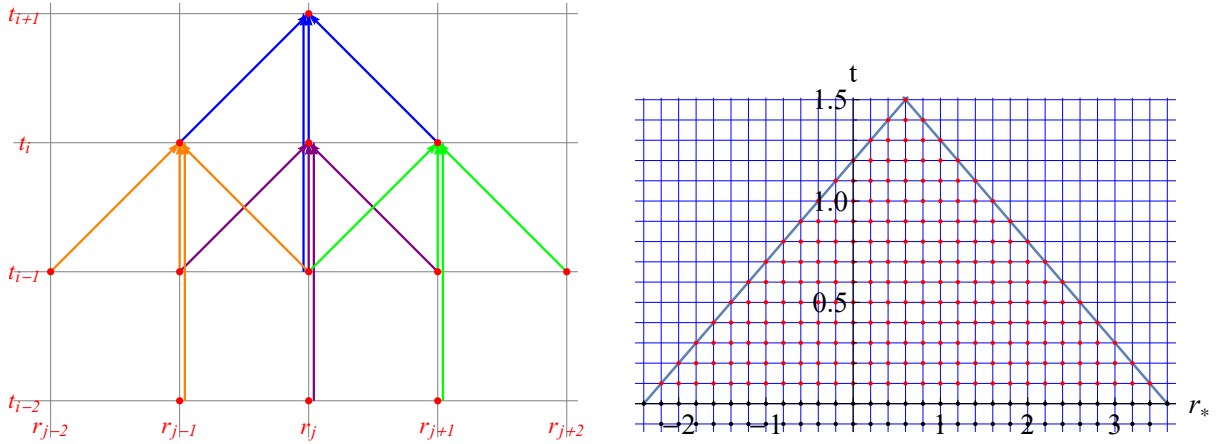


FIG. 6: The cartoon diagram of FDM. Left plot describes the descretization scheme of the coordinates (t, r_*) . Right plot describes the iterative process of the FDM. The black points are the grids to which the initial conditions are assigned. Then, the red points can be evaluated by the iterative process (Eq.(15)).

Using the FDM described above, we implement the dynamical evolution of the scalar field for $\lambda = 2$ and $\lambda = 8$ shown in Fig.7. It is clearly observed that there is two stages of the whole evolution: the Schwarzschild-like ringing phase and the de Sitter phase. The Schwarzschild-like ringing phase exhibits an oscillatory tail enveloped by a universal power law decay. While the de Sitter phase is characterized by exponential tail following the decay law:

$$|\Psi| \sim |\Psi_0| + |\Psi_1| e^{-p_l t}, \quad l = 1, 2, \dots, \quad (16)$$

where p_l in the above decay law depends on the black hole parameter λ as well as the angular

number l . When λ is small (see the left plot in Fig.7 for $\lambda = 2$), after the Schwarzschild-like ringing phase, the scalar field rapidly evolves into the time independent stage. It suggests that at this stage, the first term dominates over the second term. But for large λ (see the right plot in Fig.7), there is an obvious stage following the pure exponential decay as $e^{-p_l t}$ after the Schwarzschild-like ringing phase. After that, the scalar field also evolves into the time independent stage. Therefore, we conclude that there is a larger p_l for small l leading to a more fast decay. As λ increases, p_l becomes smaller such that before entering into the time independent stage, the exponential decay obviously emerges. It indicates that the characteristic parameter λ has the imprint on the ringing tail, which is expected to be detected by future observation.

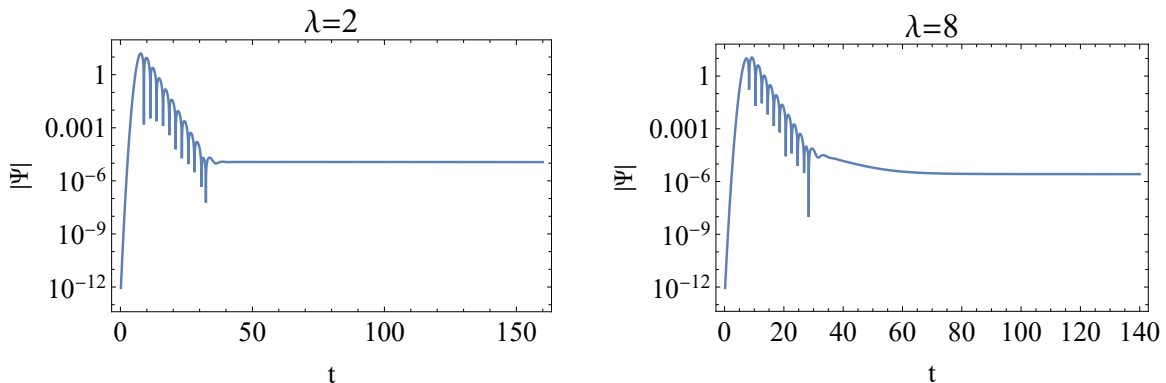


FIG. 7: Semilogarithmic plots of the dynamical evolution of scalar field for different λ . Here $l = 1$.

We would like to point out that this decay law of massless scalar field (16) has been revealed in the neutral Weyl black hole [15], comparing to which the effective dark matter ringing phase is absent in our present model. This is reasonable because in this RN-like black hole, the dark matter related term is excluded.

V. GREY-BODY FACTOR AND ENERGY EMISSION RATE

There are several approaches proposed to study the Hawking radiation for black hole. As we mentioned in the introduction, we can start from the wave equation (12) in the frequency domain to obtain the scattering coefficient from which we can obtain the grey-body factor. Then we use the grey-body factor to describe the transmission of particles through the potential, and thus work out the energy radiation rate. From the above description, in the

study we should allow the incoming waves from infinity, such that we evaluate the fraction of particles reflected back from the effective potential barrier to the event horizon. Therefore, in contrary to the QNM case, we shall impose the following scattering boundary conditions for Eq.(12)

$$\Phi = T e^{-i\omega r_*}, \quad r_* \rightarrow -\infty, \quad (17)$$

$$\Phi = e^{-i\omega r_*} + R e^{i\omega r_*}, \quad r_* \rightarrow \infty, \quad (18)$$

where T and R are the transmission and reflection coefficients, respectively. They satisfy

$$|T|^2 + |R|^2 = 1. \quad (19)$$

Then, we apply the WKB method to evaluate the reflection coefficient:

$$R = (1 + e^{-2i\pi\mathcal{K}})^{-1/2}. \quad (20)$$

\mathcal{K} in the above expression is determined by

$$\mathcal{K} = i \frac{\omega^2 - V_0}{\sqrt{-2V_2}} - \sum_{k=2}^{k=6} \Lambda_k(\mathcal{K}), \quad (21)$$

where V_0 and V_2 are the maximal value of the effective potential and its second derivative with respect to r_* at the position of the maximum, respectively. $\Lambda_k(\mathcal{K})$ are the higher WKB correction terms, which only depend on \mathcal{K} and the derivative of the effective potential at the position of its maximum. For the details, please refer to Refs.[55, 60, 61] and also appendix A. Here, we evaluate the WKB approach up to the 6th order. Then, one can work out the grey-body factor $|A_l|$ for each angular number l

$$|A_l|^2 = 1 - |R|^2 = |T|^2. \quad (22)$$

With the grey-body factor at hand, we can study the energy emission rate. We assume that the Hawking temperature of the black hole does not change between the emissions of two consequent particles, which corresponds to the canonical ensemble [62]. Then, the energy emission rate has the form [63]:

$$\frac{dE}{dt} = \sum_l N_l |A_l|^2 \frac{\omega}{\exp(\omega/T_H) - 1} \frac{d\omega}{2\pi}. \quad (23)$$

N_l are the multiplicities satisfying $N_l = 2l + 1$ for the scalar field.

The numerical results of the grey-body factor and the Hawking radiation are shown in Figs.8 and 9. We summarize the main properties as what follows.

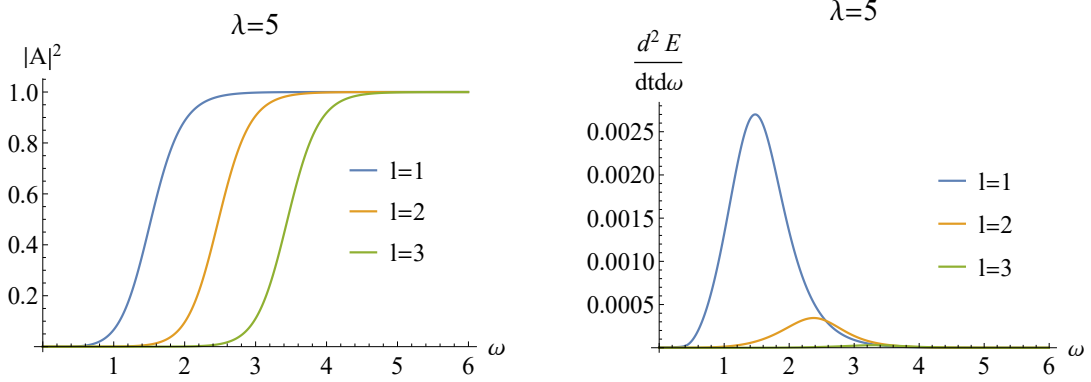


FIG. 8: The grey-body factor (left plots) and the Hawking radiation (right plots) as the function of ω for fixed λ and different l .

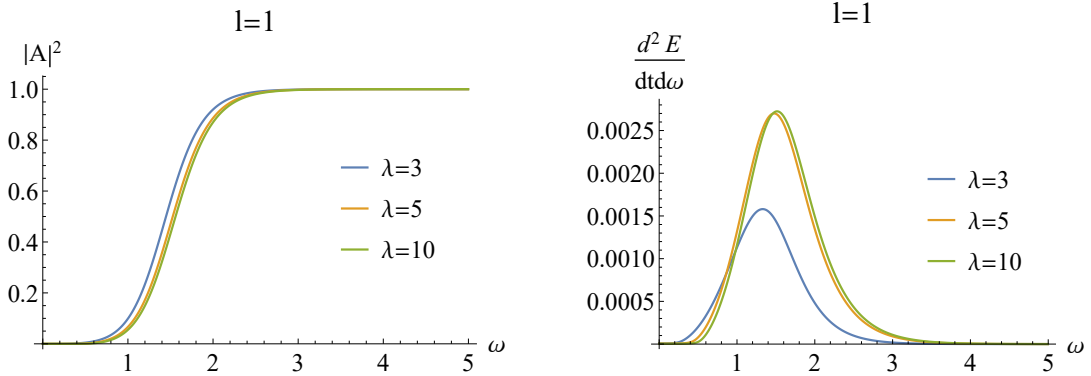


FIG. 9: The grey-body factor (left plots) and the Hawking radiation (right plots) as the function of ω for fixed l and different λ .

- As the frequency ω increases, the grey-body factor grows from almost zero to the unit. It is because when the particles possess larger energy, the probability that penetrating the potential barrier increases.
- In the intermediate frequency region, we can obviously see that for fixed frequency, the smaller is the angular number, the larger is the grey-body factor (left plots in Fig.8). It is because the effective potential has higher barrier for larger l (see Fig.3), which makes it harder for the particles to penetrate the potential barrier forming the transmission of radiation.

- With increasing λ , the grey-body factor slightly decreases for fixed frequency when the frequency is in the intermediate frequency region (left plots in Fig.9). This result can be also explained by the effective potential as argued in the above point (Fig.3).
- The energy emission rate of Hawking radiation is dominated by the modes with lower l . The contribution from the modes with higher l is virtually invisible (see the right plot in Fig.8). For fixed l , the energy emission rate of Hawking radiation grows with increasing λ . But when λ is large, the energy emission rate is almost the same (the right plot in Fig. 9).

VI. CONCLUSION AND DISCUSSION

In this paper, we study the properties of QNMs, dynamical evolution and Hawking radiation of a charged Weyl black hole by a probe massless scalar field. Firstly, by observing the effective potential of the scalar field, we find that for $l = 0$, there is a negative gap in the effective potential, which suggests a possible signal of instability. Then, we study the dynamical evolution and the QNM spectra for $l = 0$. It is observed that for the mode with $l = 0$, the scalar field grows with time and the imaginary part of QNM spectra is always positive. It confirms that the mode with $l = 0$ is really unstable under the perturbation of scalar field. Therefore, we mainly focus on the properties of QNM spectra, dynamical evolution and Hawking radiation for the modes with $l > 0$. We summarize the main properties as what follows.

- The absolute value of the real part of QNM frequency grows with λ , which means that the oscillation of the dynamical perturbation increases with λ . Especially, we find that both the real and imaginary parts of the QNM frequencies approach a constant when λ is large enough.
- The dynamical evolution of the scalar field consists of two stages: the Schwarzschild-like ringing phase and the de Sitter phase. The effective dark matter ringing phase observed in the neutral Weyl black hole is absent in this charged Weyl black hole background. It can attribute to the dark matter related term is excluded in our present model.

- In the low frequency region, the grey-body factor vanishes. As the frequency ω increases, the grey-body grows, and approaches the unit in the high frequency region. This picture is independent of the black hole parameter and the angular number. It can be explained as that in the low or high frequency region, the effect from the energy dominates over that from the black hole parameter and the angular number.
- Correspondingly, the Hawking radiation increases with increasing ω at first, and then decreases after climbing up a maximum. In addition, with the increase of λ , the Hawking radiation grows, and approaches a constant when λ is large enough.

Acknowledgments

This work is supported by National Key R&D Program of China (No. 2020YFC2201400), the Natural Science Foundation of China under Grants No. 12035005, 11905083, 11775036, 12147209, and Fok Ying Tung Education Foundation under Grant No. 171006. X.-M.K. is also supported by Natural Science Foundation of Jiangsu Province under Grant No. BK20211601. J.-P.W. is also supported by Top Talent Support Program from Yangzhou University.

Appendix A: WKB method and error estimation

There are several methods determining the QNMs. WKB method is a widely-used and economic semianalytic method to solve the eigenvalue problem. However, the WKB formula usually gives a best accuracy for $l > n$ [55, 56]. When $l \leq n$, this method does not always give a reliable result [55, 56]. In addition, increasing the WKB order does not always give a better approximation for the QNM spectra. Sometimes higher-order formula increases the error [55, 56].

For a wave-like equation with a potential barrier, when the two turning points close enough, the potential function can be expanded by the Taylor series at the position of the peak of the potential. The key point of WKB method is to match the exterior WKB solutions across the two turning points. Therefore, the validity of this method relies heavily upon the form of the effective potential.

The 1st order WKB was first proposed by Schutz and Will [61]. Then, Iyer and Will

developed the 3rd order WKB method [64, 65]. The accuracy of the 3rd WKB for the fundamental mode has reached about 1%. Soon afterwards, the WKB method was extended to the 6th order by Konoplya [55, 66] and 13th order by Matyjasek and Opala [67].

Usually, we have the following general higher order WKB formula [56]

$$\omega^2 = V_0 + \Lambda_2(\mathcal{K}^2) + \Lambda_4(\mathcal{K}^2) + \dots - i\mathcal{K}\sqrt{-2V_2}(1 + \Lambda_3(\mathcal{K}^2) + \Lambda_5(\mathcal{K}^2) + \dots), \quad (\text{A1})$$

where \mathcal{K} takes half-integer value. $\Lambda_k(\mathcal{K}^2)$ is the k th order correction term, which depends on the derivative of the effective potential at the position of its maximum. V_i denotes the derivative with respect with r at the position of its maximum. Notice that V_0 is the potential itself at the position of its maximum.

In order to further improve the accuracy, we consider the WKB formula proposed by Matyjasek and Opala [67] and use Padé approximant. Then, the WKB formula (A1) can be reformulated as

$$P_k(\epsilon) = V_0 + \Lambda_2(\mathcal{K}^2)\epsilon^2 + \Lambda_4(\mathcal{K}^2)\epsilon^4 + \dots - i\mathcal{K}\sqrt{-2V_2}(1 + \Lambda_3(\mathcal{K}^2)\epsilon^3 + \Lambda_5(\mathcal{K}^2)\epsilon^5 + \dots). \quad (\text{A2})$$

$P_k(\epsilon)$ called Padé approximant are polynomials of a family of the rational functions

$$P_{\tilde{n}/\tilde{m}}(\epsilon) = \frac{Q_0 + Q_1\epsilon + \dots + Q_{\tilde{n}}\epsilon^{\tilde{n}}}{R_0 + R_1\epsilon + \dots + R_{\tilde{m}}\epsilon^{\tilde{m}}} \quad (\text{A3})$$

with $\tilde{n} + \tilde{m} = k$. The squared frequency is obtained for $\epsilon = 1$, i.e., $\omega^2 = P_k(1)$. The improved WKB method with Padé approximant provides a more powerful tool with higher accuracy to find QNMs, especially for $\tilde{n} \approx \tilde{m} \approx k/2$ [56, 67].

To estimate the error of the WKB approximantion, we define the quantity [56]

$$\Delta_k = \frac{|\omega_{k+1} - \omega_{k-1}|}{2}. \quad (\text{A4})$$

Then, we can use the following inequation to evaluate the error order [56]

$$\Delta_k \gtrsim |\omega - \omega_k|, \quad (\text{A5})$$

where ω is the accurate value of the QNM frequency.

The plots above in Fig.10 show the real and imaginary parts of the dominant frequency ($n = 0$) for different WKB orders. We see that both the real and imaginary parts of the QNM frequency are convergent as the WKB order increases. Especially, we find that for

our model studied here, it is best to calculate the QNM frequency is the 6th-order WKB approximation, which allows the error estimation less than 0.1%.

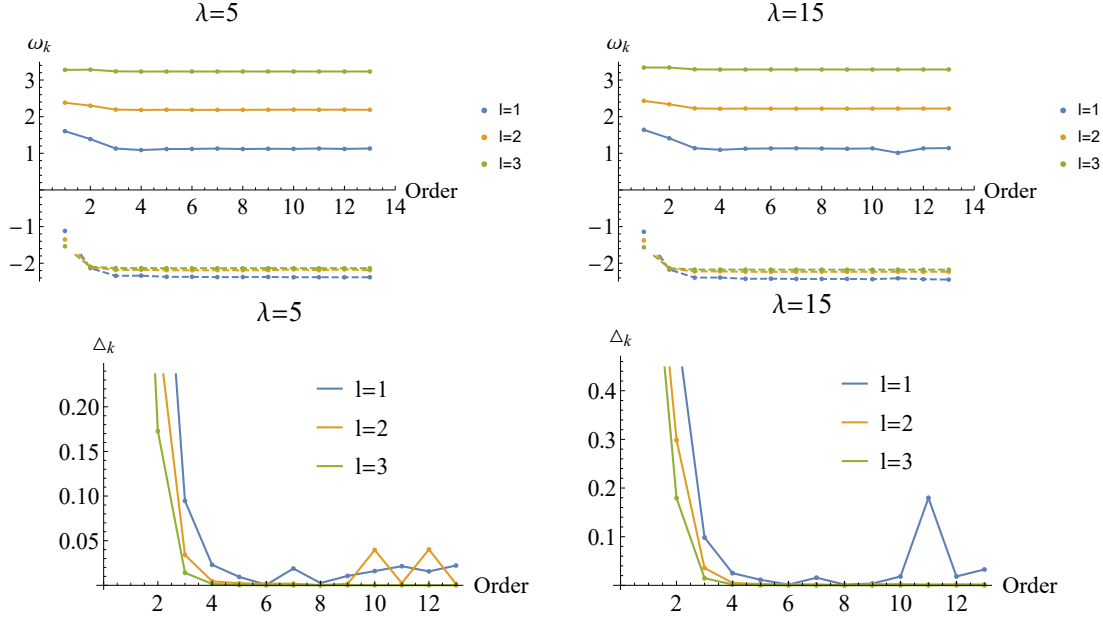


FIG. 10: The plots above: The real part (solid lines) and imaginary part (dashed line) of the dominant frequency ($n = 0$) for different WKB orders. The plots below: The error Δ_k for different WKB orders.

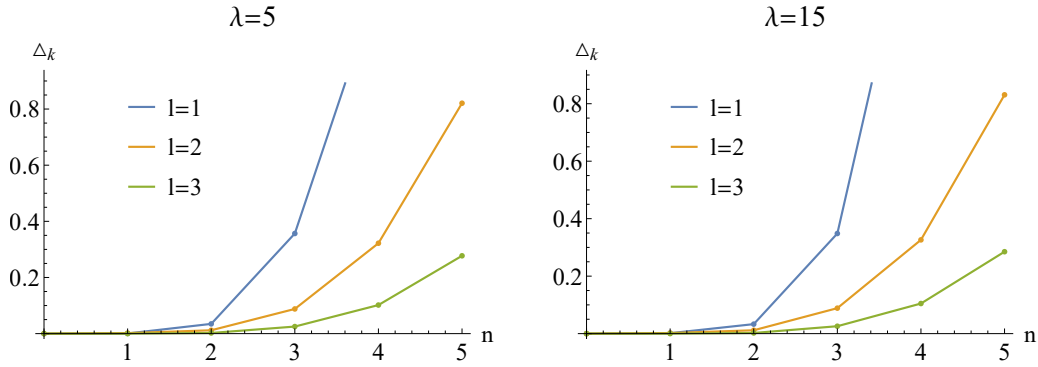


FIG. 11: The error Δ_k v.s. the overtone number n for the 6th-order WKB.

In addition, we also show the error estimation Δ_k v.s. the overtone number n for the 6th-order WKB in Fig.(11). We find that with increasing n for fixed l , the error estimation Δ_k rapidly increases and the WKB method loses its power to find the accurate QNMs.

Therefore, the WKB method applies only for $l > n$, which is also pointed out in [56].

-
- [1] **LIGO Scientific, Virgo** Collaboration, B. P. Abbott et al., *Observation of Gravitational Waves from a Binary Black Hole Merger*, Phys. Rev. Lett. **116** (2016), no. 6 061102, [[arXiv:1602.03837](#)].
 - [2] **LIGO Scientific, Virgo** Collaboration, B. P. Abbott et al., *Tests of general relativity with GW150914*, Phys. Rev. Lett. **116** (2016), no. 22 221101, [[arXiv:1602.03841](#)]. [Erratum: Phys. Rev. Lett. **121** (2018) 129902].
 - [3] **LIGO Scientific, Virgo** Collaboration, B. P. Abbott et al., *GW151226: Observation of Gravitational Waves from a 22-Solar-Mass Binary Black Hole Coalescence*, Phys. Rev. Lett. **116** (2016), no. 24 241103, [[arXiv:1606.04855](#)].
 - [4] **Event Horizon Telescope** Collaboration, K. Akiyama et al., *First M87 Event Horizon Telescope Results. I. The Shadow of the Supermassive Black Hole*, Astrophys. J. Lett. **875** (2019) L1, [[arXiv:1906.11238](#)].
 - [5] **Event Horizon Telescope** Collaboration, K. Akiyama et al., *First M87 Event Horizon Telescope Results. IV. Imaging the Central Supermassive Black Hole*, Astrophys. J. Lett. **875** (2019), no. 1 L4, [[arXiv:1906.11241](#)].
 - [6] **Event Horizon Telescope** Collaboration, K. Akiyama et al., *First Sagittarius A* Event Horizon Telescope Results. I. The Shadow of the Supermassive Black Hole in the Center of the Milky Way*, Astrophys. J. Lett. **930** (2022), no. 2 L12.
 - [7] **Event Horizon Telescope** Collaboration, K. Akiyama et al., *First Sagittarius A* Event Horizon Telescope Results. VI. Testing the Black Hole Metric*, Astrophys. J. Lett. **930** (2022), no. 2 L17.
 - [8] H. Weyl, *Reine In nitesimalgeometrie*, Math. Z. **2** (1918), no. 3-4 384–411.
 - [9] K. S. Stelle, *Renormalization of higher-derivative quantum gravity*, Phys. Rev. D **16** (Aug, 1977) 953–969.
 - [10] F. F. Faria, *Quantum massive conformal gravity*, Eur. Phys. J. C **76** (2016), no. 4 188, [[arXiv:1503.04355](#)].
 - [11] *Extended conformal supergravity*, Nucl. Phys. B **182** (1981), no. 1 173–204.
 - [12] B. de Wit, J. W. van Holten, and A. Van Proeyen, *Structure of N=2 Supergravity*, Nucl.

- Phys. B **184** (1981) 77. [Erratum: Nucl. Phys. B **222** (1983) 516].
- [13] J. Maldacena, *Einstein Gravity from Conformal Gravity*, [arXiv:1105.5632](#).
 - [14] G. Anastasiou and R. Olea, *From conformal to Einstein Gravity*, Phys. Rev. D **94** (2016), no. 8 086008, [[arXiv:1608.07826](#)].
 - [15] R. A. Konoplya, *Conformal Weyl gravity via two stages of quasinormal ringing and late-time behavior*, Phys. Rev. D **103** (2021), no. 4 044033, [[arXiv:2012.13020](#)].
 - [16] P. D. Mannheim and D. Kazanas, *Exact Vacuum Solution to Conformal Weyl Gravity and Galactic Rotation Curves*, Astrophys. J. **342** (1989) 635–638.
 - [17] P. D. Mannheim, *Alternatives to dark matter and dark energy*, Prog. Part. Nucl. Phys. **56** (2006) 340–445, [[astro-ph/0505266](#)].
 - [18] R. Nesbet, *Conformal Gravity: Dark Matter and Dark Energy*, Entropy **15** (Jan., 2013) 162–176, [[arXiv:1208.4972](#)].
 - [19] P. D. Mannheim and D. Kazanas, *Solutions to the Kerr and Kerr-Newman problems in fourth order conformal Weyl gravity*, Phys. Rev. D **44** (1991) 417–423.
 - [20] M. R. Tanhayi, M. Fathi, and M. V. Takook, *Observable Quantities in Weyl Gravity*, Mod. Phys. Lett. A **26** (2011) 2403–2410, [[arXiv:1108.6157](#)].
 - [21] F. Payandeh and M. Fathi, *Spherical Solutions due to the Exterior Geometry of a Charged Weyl Black Hole*, Int. J. Theor. Phys. **51** (2012) 2227–2236, [[arXiv:1202.2415](#)].
 - [22] E. Berti, V. Cardoso, and A. O. Starinets, *Quasinormal modes of black holes and black branes*, Class. Quant. Grav. **26** (2009) 163001, [[arXiv:0905.2975](#)].
 - [23] E. Berti, V. Cardoso, and C. M. Will, *On gravitational-wave spectroscopy of massive black holes with the space interferometer LISA*, Phys. Rev. D **73** (2006) 064030, [[gr-qc/0512160](#)].
 - [24] E. Berti, K. Yagi, H. Yang, and N. Yunes, *Extreme Gravity Tests with Gravitational Waves from Compact Binary Coalescences: (II) Ringdown*, Gen. Rel. Grav. **50** (2018), no. 5 49, [[arXiv:1801.03587](#)].
 - [25] S. W. Hawking, *Particle Creation by Black Holes*, Commun. Math. Phys. **43** (1975) 199–220.
 - [26] D. N. Page, *Particle emission rates from a black hole: Massless particles from an uncharged, nonrotating hole*, Phys. Rev. D **13** (Jan, 1976) 198–206.
 - [27] C. M. Harris and P. Kanti, *Hawking radiation from a $(4+n)$ -dimensional black hole: Exact results for the Schwarzschild phase*, JHEP **10** (2003) 014, [[hep-ph/0309054](#)].
 - [28] C.-Y. Zhang, P.-C. Li, and M. Guo, *Greybody factor and power spectra of the Hawking*

- radiation in the 4D Einstein–Gauss–Bonnet de-Sitter gravity*, Eur. Phys. J. C **80** (2020), no. 9 874, [[arXiv:2003.13068](#)].
- [29] R. A. Konoplya, A. F. Zinhailo, and Z. Stuchlik, *Quasinormal modes, scattering, and Hawking radiation in the vicinity of an Einstein-dilaton-Gauss-Bonnet black hole*, Phys. Rev. D **99** (2019), no. 12 124042, [[arXiv:1903.03483](#)].
- [30] R. A. Konoplya and A. F. Zinhailo, *Hawking radiation of non-Schwarzschild black holes in higher derivative gravity: a crucial role of grey-body factors*, Phys. Rev. D **99** (2019), no. 10 104060, [[arXiv:1904.05341](#)].
- [31] R. A. Konoplya, A. F. Zinhailo, and Z. Stuchlik, *Quasinormal modes and Hawking radiation of black holes in cubic gravity*, Phys. Rev. D **102** (2020), no. 4 044023, [[arXiv:2006.10462](#)].
- [32] R. A. Konoplya and A. F. Zinhailo, *Grey-body factors and Hawking radiation of black holes in 4D Einstein-Gauss-Bonnet gravity*, Phys. Lett. B **810** (2020) 135793, [[arXiv:2004.02248](#)].
- [33] R. A. Konoplya, *Black holes in galactic centers: Quasinormal ringing, grey-body factors and Unruh temperature*, Phys. Lett. B **823** (2021) 136734, [[arXiv:2109.01640](#)].
- [34] H. Guo, H. Liu, X.-M. Kuang, and B. Wang, *Acoustic black hole in Schwarzschild spacetime: quasi-normal modes, analogous Hawking radiation and shadows*, Phys. Rev. D **102** (2020) 124019, [[arXiv:2007.04197](#)].
- [35] R. Ling, H. Guo, H. Liu, X.-M. Kuang, and B. Wang, *Shadow and near-horizon characteristics of the acoustic charged black hole in curved spacetime*, Phys. Rev. D **104** (2021), no. 10 104003, [[arXiv:2107.05171](#)].
- [36] W.-C. Syu, D.-S. Lee, and C.-Y. Lin, *Analogous Hawking radiation and quantum entanglement in two-component Bose-Einstein condensates: the gapped excitations*, [arXiv:2204.10790](#).
- [37] M. Fathi, M. Kariminezhad, M. Olivares, and J. R. Villanueva, *Motion of massive particles around a charged Weyl black hole and the geodetic precession of orbiting gyroscopes*, Eur. Phys. J. C **80** (2020), no. 5 377, [[arXiv:2009.03399](#)].
- [38] M. Fathi, M. Olivares, and J. R. Villanueva, *Classical tests on a charged Weyl black hole: bending of light, Shapiro delay and Sagnac effect*, Eur. Phys. J. C **80** (2020), no. 1 51, [[arXiv:1910.12811](#)].
- [39] M. Fathi and J. R. Villanueva, *The role of elliptic integrals in calculating the gravitational*

- lensing of a charged Weyl black hole surrounded by plasma*, [arXiv:2009.03402](#).
- [40] M. Fathi, M. Olivares, and J. R. Villanueva, *Gravitational Rutherford scattering of electrically charged particles from a charged Weyl black hole*, Eur. Phys. J. Plus **136** (2021), no. 4 420, [[arXiv:2009.03404](#)].
 - [41] S. Chandrasekhar, *The mathematical theory of black holes. Oxford classic texts in the physical sciences*, Oxford Univ. Press, Oxford (2002).
 - [42] H.-P. Nollert, *TOPICAL REVIEW: Quasinormal modes: the characteristic ‘sound’ of black holes and neutron stars*, Class. Quant. Grav. **16** (1999) R159–R216.
 - [43] R. A. Konoplya and A. Zhidenko, *Quasinormal modes of black holes: From astrophysics to string theory*, Rev. Mod. Phys. **83** (2011) 793–836, [[arXiv:1102.4014](#)].
 - [44] K. D. Kokkotas and B. G. Schmidt, *Quasinormal modes of stars and black holes*, Living Rev. Rel. **2** (1999) 2, [[gr-qc/9909058](#)].
 - [45] J. P. Boyd, *Chebyshev & Fourier Spectral Methods*, Courier Dover Publications.
 - [46] A. Jansen, *Overdamped modes in Schwarzschild-de Sitter and a Mathematica package for the numerical computation of quasinormal modes*, Eur. Phys. J. Plus **132** (2017), no. 12 546, [[arXiv:1709.09178](#)].
 - [47] J.-P. Wu and P. Liu, *Quasi-normal modes of holographic system with Weyl correction and momentum dissipation*, Phys. Lett. B **780** (2018) 616–621, [[arXiv:1804.10897](#)].
 - [48] G. Fu and J.-P. Wu, *EM Duality and Quasinormal Modes from Higher Derivatives with Homogeneous Disorder*, Adv. High Energy Phys. **2019** (2019) 5472310, [[arXiv:1812.11522](#)].
 - [49] W. Xiong, P. Liu, C.-Y. Zhang, and C. Niu, *Quasi-normal modes of the Einstein-Maxwell-aether Black Hole*, [arXiv:2112.12523](#).
 - [50] P. Liu, C. Niu, and C.-Y. Zhang, *Linear instability of charged massless scalar perturbation in regularized 4D charged Einstein-Gauss-Bonnet anti de-Sitter black holes*, Chin. Phys. C **45** (2021), no. 2 025111.
 - [51] P. Liu, C. Niu, and C.-Y. Zhang, *Instability of regularized 4D charged Einstein-Gauss-Bonnet de-Sitter black holes*, Chin. Phys. C **45** (2021), no. 2 025104.
 - [52] J. L. Jaramillo, R. Panosso Macedo, and L. Al Sheikh, *Pseudospectrum and Black Hole Quasinormal Mode Instability*, Phys. Rev. X **11** (2021), no. 3 031003, [[arXiv:2004.06434](#)].
 - [53] J. L. Jaramillo, R. Panosso Macedo, and L. A. Sheikh, *Gravitational wave signatures of black hole quasi-normal mode instability*, [arXiv:2105.03451](#).

- [54] K. Destounis, R. P. Macedo, E. Berti, V. Cardoso, and J. L. Jaramillo, *Pseudospectrum of Reissner-Nordström black holes: Quasinormal mode instability and universality*, Phys. Rev. D **104** (2021), no. 8 084091, [[arXiv:2107.09673](#)].
- [55] R. A. Konoplya, *Quasinormal behavior of the d-dimensional Schwarzschild black hole and higher order WKB approach*, Phys. Rev. D **68** (2003) 024018, [[gr-qc/0303052](#)].
- [56] R. A. Konoplya, A. Zhidenko, and A. F. Zinhailo, *Higher order WKB formula for quasinormal modes and grey-body factors: recipes for quick and accurate calculations*, Class. Quant. Grav. **36** (2019) 155002, [[arXiv:1904.10333](#)].
- [57] E. Abdalla, C. E. Pellicer, J. de Oliveira, and A. B. Pavan, *Phase transitions and regions of stability in reissner-nordström holographic superconductors*, Phys. Rev. D **82** (2010) 124033, [[arXiv:1010.2806](#)].
- [58] Z. Zhu, S.-J. Zhang, C. E. Pellicer, B. Wang, and E. Abdalla, *Stability of reissner-nordström black hole in de sitter background under charged scalar perturbation*, Phys. Rev. D **90** (2014), no. 4 044042, [[arXiv:1405.4931](#)]. [Addendum: Phys. Rev. D 90 (2014) 049904].
- [59] K. Lin and W.-L. Qian, *Echoes in star quasinormal modes using an alternative finite difference method*, [arXiv:2204.09531](#).
- [60] S. Iyer and C. M. Will, *Black-hole normal modes: A wkb approach. i. foundations and application of a higher-order wkb analysis of potential-barrier scattering*, Phys. Rev. D **35** (Jun, 1987) 3621–3631.
- [61] B. Schutz and C. Will, *Black hole normal modes - A semianalytic approach*, Astrophys. J. Lett , Astrophys. J. Lett **291** (Apr., 1985) L33–L36.
- [62] P. Kanti, *Black holes in theories with large extra dimensions: A Review*, Int. J. Mod. Phys. A **19** (2004) 4899–4951, [[hep-ph/0402168](#)].
- [63] S. W. Hawking, *Particle Creation by Black Holes*, Commun. Math. Phys. **43** (1975) 199–220. [Erratum: Commun. Math. Phys. **46** (1976) 206].
- [64] S. Iyer and C. M. Will, *Black Hole Normal Modes: A WKB Approach. 1. Foundations and Application of a Higher Order WKB Analysis of Potential Barrier Scattering*, Phys. Rev. D **35** (1987) 3621.
- [65] J. W. Guinn, C. M. Will, Y. Kojima, and B. F. Schutz, *High Overtone Normal Modes of Schwarzschild Black Holes*, Class. Quant. Grav. **7** (1990) L47.
- [66] R. A. Konoplya, *Quasinormal modes of the Schwarzschild black hole and higher order WKB*

- approach*, J. Phys. Stud. **8** (2004) 93–100.
- [67] J. Matyjasek and M. Opala, *Quasinormal modes of black holes. The improved semianalytic approach*, Phys. Rev. D **96** (2017), no. 2 024011, [[arXiv:1704.00361](#)].